Texture-enhanced detection of tropical deforestation using ALOS-PALSAR

MartinWhittle and Shaun Quegan

CTCD, University of Sheffield, Hicks Building, Hounsfield Rd, Sheffield S3 7RH

Keywords: Forest monitoring, tropical deforestation, change detection, texture, ALOS PALSAR

Abstract

The development of reliable forest monitoring systems in tropical regions is crucial to support initiatives designed to limit the spread of deforestation. Optical monitoring in is hampered by the frequent cloud cover in tropical regions, but this is not a problem for space-borne Synthetic Aperture Radar (SAR) systems. We have previously developed techniques of using L-band SAR data from the JAXA Advanced Land Observing Satellite (ALOS) able to detect 70% of deforestation at a false alarm rate of 20%. In this paper we build on that work to show that the introduction of textural measures can boost the equivalent detection rate to 82%. We also extend the study to discuss the transferability of these results to adjacent regions.

1. Introduction

Tropical forests support rich, bio-diverse habitats and have a complex influence on climate through physical, chemical and biological processes(Bonan 2008; Pitman et al. 2004), but they are under huge pressure worldwide from agriculture clearance and logging for their resources(DeFries et al. 2010). Deforestation not only destroys these remaining natural habitats, it also releases carbon dioxide and reduces its uptake by plants. However, forests also buffer climate extremes and help to maintain the hydrological cycle. These feedbacks are currently under-represented in the development of policy which usually focuses simply on reducing greenhouse gasses(McAlpine et al. 2010). Land-use changes, dominated by deforestation and associated burning, are responsible for almost a quarter of all anthropogenic carbon emissions (FAQ7.1.(IPCC 2007). The Reducing Emissions from Deforestation and forest Degradation (REDD/REDD+) mechanism (http://www.un-redd.org/) established under the United Nations Framework Convention on Climate Change (UNFCCC) seeks to encourage developing countries to curb deforestation, foster carbon stocks and reverse the trend by offering financial incentives. However, the large degree of uncertainty in estimates of deforestation rates and the associated emissions (Achard et al. 2002; Houghton 2005, 2010; Le Quéré 2010) weaken the argument for the need to change and impede the implementation of controls. Reducing this uncertainty is crucial to assessments of global carbon balance for climate modelling and harnessing political will for change. are also dependent on reliable, independent estimations of deforestation rates (Goetz et al. 2009). Hence, the REDD+ initiative also encourages countries to develop forest monitoring systems as part of a drive towards sustainability and improved carbon accounting. RREF (COP16/CMP6 2010). Major forests cover vast, remote areas and efficient monitoring techniques are therefore largely dependent on satellite-based techniques. In humid tropical regions the frequent and extensive cloud cover is a major handicap to optical-based systems and methods are being sought to develop radar-based techniques using cloud-piercing frequencies. The Japanese Aerospace Exploration Agency (JAXA) Advanced Land Observing Satellite "Daichi" (ALOS) (Rosenqvist et al. 2007) was fully operational between June 2006 and April 2011 when it suffered a power failure. It included a Phased Array L-band Synthetic Aperture Radar (PALSAR) operating at 1270 MHz (a wavelength of 26.4 cm) and provided a number of image products. In a recent publication(Whittle et al. 2011) we developed and evaluated techniques of

using Synthetic Aperture Radar (SAR) imagery from ALOS to detect deforestation in tropical forests using the Riau region of Sumatra as an example.

Indonesia has the third most extensive tropical forest cover in the world, much of it covering peatland that can hold more CO_2 than the forest itself(Hooijer et al. 2010; Page et al. 2002). However, Indonesia's current deforestation rate of 3.4% per year is second only to that of Brazil among countries with humid tropical forests (Hansen et al. 2009; Hansen et al. 2008). Sumatra has the most intense recent large-scale forest clearance in Indonesia, with the province of Riau recording the highest degree of change (Broich et al. 2011; Hansen et al. 2009). Deforestation in Indonesia ranges from selective logging to large-scale clearance for pulp wood and agricultural plantations to slash and burn clearance. In line with REDD proposals monitoring is urgently needed for independent verification(Fuller 2006) .

The earlier paper{Whittle, 2012 #70} used a case study in Riau to develop methods of detecting deforestation using SAR data from the ALOS satellite. Using the available databases(Uryu et al. 2010) we focussed solely on the regions that were forested in mid-2007 and compared with the later database to determine which regions were deforested by mid-2008. We used two ALOS products in different ways and found that it was advantageous to combine the results of both. ScanSAR images are single-polarized products acquired with the same geometry once every 46 days with a resolution of 100 m. They typically cover 359 km in range and 379 km in swath, i.e. 136000 km^2, and are potentially well suited to monitoring applications. We obtained time-series of these and found that the temporal standard deviation, *SD*, was the best indicator of deforestation over the period of the study. Fine Beam Dual (FBD) images are obtained with HH & HV polarization at a resolution of 12.5 m. They have dimensions of 69.8 km in range by 58.6 km in azimuth, with repeat images usually acquired at 3 times a year during June, July and September. We developed a ratio technique for the analysis of intensity changes between pairs of time-separated FBD images. We also found that the temporal analysis of a time series of lower resolution ScanSAR images could give comparable results but was compromised by strong temporal fluctuations in backscatter, probably due to significant precipitation and flooding events since they often highlighted river basins. Combination of both types of data using data fusion techniques gave a 10% improvement in the detection rates.

SAR images are obtained using coherent radiation and include an element of speckle caused by interference from adjacent scattering centres. Much of this speckle is filtered from our images before analysis and the resulting image texture is related to scene texture that represents variations in the locally averaged reflectivity on the scale of the wavelength used(Raney 1998); it therefore potentially contains useful information about land cover. Image texture describes variations in the intensity over neighbouring pixels and a number of measures can be derived from second order statistics(Oliver and Quegan 2004). It has previously been demonstrated that such texture measures can be used to distinguish between forest and non-forest for c-band airborne SAR(Oliver 2000). Furthermore, since our original methods were based on first-order intensities, we may expect that these second-order measures could provide extra information that might usefully be combined with the original techniques. In this paper we compare and evaluate two basic texture measures, individually and in combination, as indicators of deforestation with previously developed techniques. We

also extend the previous study to another three FBD scenes and discuss the transferability of results.

2. Data

2.1 Study areas: ground and satellite data coverage

FBD data were acquired for the dates shown in Table 1 for four scenes (identified by path, P, and frame number, F) over the Riau province of Sumatra as shown in Figure 1. We also used two adjacent sets of 12 ScanSAR images each, acquired at intervals of 46 days between 31/01/2007 and 20/06/2008. These cover the FBD scenes as shown in Figure 1. All data were multi-channel filtered (Quegan and Yu 2001) before use. RGB images of these scenes can be found in the supplementary information.

Table 1 Acquisition dates for the FBD data used in this study and dates for the Landsat images used to construct the databases for the same scenes used in the analysis.

Scene	FBD		Databases	
	1st image	2nd image	nf2007	nf08-09
P443-F7170	28/06/2007	30/06/2008	23/04/2007 14/11/2006	22/07/2008, 24/09/2008
P443-F7180	28/06/2007	30/06/2008	Exact dates unavailable	22/07/2008
P443-F7190	28/06/2007	30/06/2008	Exact dates unavailable	22/07/2008
P445-F7170	01/08/2007	03/05/2008	Exact dates unavailable	18/05/2008, 22/07/2008, 11/06/2008, 24/09/2008

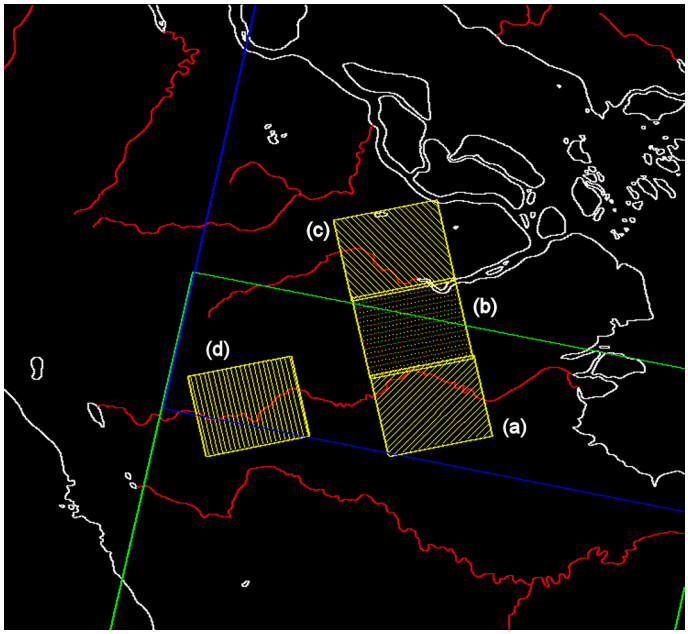

Figure 1. The four FBD scenes (hatched yellow) superimposed on an outline of central Sumatra (white) with rivers (red). (a) P443-F7170; (b) P443-F7180; (c) P443-F7190; (d) P445-F7170. Partial outlines of the two ScanSAR scenes used are also shown: P115-F3650 (green) and P115-F3600 (blue).

The earlier work(Whittle et al. 2011) used a detailed land cover database, WWF2007, that covered the Riau region and a prototype database that distinguished only natural forest and non-forest for part of Riau nominally dated 2008. Both databases were based on the interpretation of Landsat imagery. These have since been incorporated into more extensive databases, WWF-nf2007 and WWF-nf08-09, which delineate only forest and non-forest but cover the whole of Sumatra. Over the regions studied here the Landsat imagery was acquired during mid-2008 (Table 1). However, the Landsat footprints do not correspond with the FBD scenes and exact dates for the database therefore cannot be defined for two of the scenes used. These databases have also undergone some manual correction and consequently vary slightly from the earlier versions over the regions studied here. Table 2 shows the degree of overlap between the old and new versions of the databases for 2008 for the scene P443_F7170. The natural forest indicated as lost between the nf2007 and nf08-09 databases is used as our reference for deforestation in this work. These show that the new 2008 database has 2% less natural forest than the original version but the location of forest has also changed giving a reduction of 4.6% in the overlap between old and new. As a consequence the deforested region according to the new database is reduced by <1% but changes in location have led to a difference in overlap of 6.5%. A full discussion of the effect of such errors was presented in the earlier paper(Whittle et al. 2011), here we will see that the effect of correcting the databases is that the measured detection rate is improved.

Table 2a. Overlap of natural forest regions used in the original databases (WWF2007) and the new database WWF-nf07 used in this work, for the scene P443_F7170. Values are also expressed as a fraction of the count obtained from the original database.

Counts	*nf07(new)*	*nf07(old)*	*Fraction*	*nf07(new)*	*nf07(old)*
nf07(new)	8553348	8547340	nf08(new)	1.000	0.999
nf07(old)	8547340	8552272	nf08(old)	0.999	1.000

Table 2b. Overlap of natural forest regions used in the original databases (WWF2008) and the new database WWF-nf08-09 used in this work, for the scene P443_F7170. . Values are also expressed as a fraction of the count obtained from the original database.

Counts	*nf08(new)*	*nf08(old)*	*Fraction*	*nf08(new)*	*nf08(old)*
nf08(new)	5981374	5817745	nf08(new)	0.981	0.954
nf08(old)	5817745	6096144	nf08(old)	0.954	1.000

Table 2c. Overlap of deforested regions obtained by difference between the original databases (WWF2007 and WWF2008) and the databases (WWF-nf2007 and WWF-nf08-09) used in this work, for the scene P443_F7170. . Values are also expressed as a fraction of the count obtained from the original database.

Counts	*DF(new)*	*DF(old)*	*Fraction*	*DF(new)*	*DF(old)*
DF(new)	2571974	2422624	DF(new)	0.993	0.935
DF(old)	2422624	2590280	DF(old)	0.935	1.000

3. Methods

3.1 Assessment methods

We will develop a number of different change measures which are assessed by comparison with the differences between the two databases nf07 and nf08 which we take to indicate deforestation. This procedure is subject to errors in the database and also because deforestation may have occurred between the dates of the Landsat images used to derive the 2007 database and the first FBD scene, or the dates of the second FBD image and the Landsat images used to derive the 2008 database. Both types of error have been discussed in the earlier work(Whittle et al. 2011). Change measures were evaluated as detectors of deforestation by first obtaining a probability density function (PDF) for the property in question over the known natural forest region within the scene as defined by the earlier database, nf07. The PDF was then integrated to obtain a cumulative density function (CDF). Then by comparing the pixels associated above a given percentile threshold of the CDF with the deforested and undisturbed regions known from the difference between the two databases it is possible to assign a probability of detection, P_d (the probability that a deforested pixel would be correctly detected as such), and a probability of false alarm, P_{fa} (the probability that a pixel of undisturbed forest could be wrongly flagged as deforested), for the percentile used. There is always a trade off between P_d and P_{fa} – high rates of detection can always be achieved but they come at the expense of increasing the false

alarm rate. By taking a series of percentile values and plotting the P_d against the P_{fa} a receiver operating characteristic (ROC) can be obtained, which can then be used to assess the usefulness of the detection method. It is also convenient for comparative purposes to choose values of P_{fa} that can be tolerated in practice, thus we will frequently compare results for P_{fa} = 0.1 and 0.2.

3.2 Intensity measures of change

In the original publication we used a ratio technique to detect intensity changes between time-separated FBD images. The ratio is preferred over differencing because the latter accentuates the difference in speckle(Oliver and Quegan 2004; Rignot and van Zyl 1993). After co-registering images using GAMMA software (http://www.gamma-rs.ch/) and applying a multi-channel filter (Quegan and Yu 2001) we found that both increases and decreases in intensity could be associated with deforestation events and for this reason the change measure adopted combined both sorts of change:

$$R_1(\mathbf{x}) = \max\left[\frac{I_{old}(\mathbf{x})}{I_{new}(\mathbf{x})}, \frac{I_{new}(\mathbf{x})}{I_{old}(\mathbf{x})}\right] - 1, \qquad (1)$$

where $I_{old}(\mathbf{x})$ and $I_{new}(\mathbf{x})$ are the intensities at position **x** for the earlier and later images respectively. Furthermore, we found that the HH and HV channels make significantly different contributions which could be effectively combined as the average,

$$R1 = \tfrac{1}{2}\left[R_1(HH) + R_1(HV)\right], \qquad (2)$$

to make worthwhile improvements in the detection of deforestation. In the earlier paper(Whittle et al. 2011) this term was called R_1^{av}, in this paper it is labelled $R1$ to simplify notation.

3.3 Multi-temporal ScanSAR detection

We previously found that the temporal standard deviation *SD* was the multi-temporal measure of change that gave the best detection rates of deforestation. The ScanSAR images were first co-registered using GAMMA software and a multi-channel filter (Quegan and Yu 2001) was applied with window size 5×5 to reduce speckle. The nf07 database was used to prepare forest masks for each of the four FBD scenes. These were used to find the mean forest backscatter $\bar{I}_f(k)$ for each ScanSAR image, *k*, over each FBD footprint. The data was then rescaled so that the mean forest intensity in each image became equal to the time-average of the overall mean forest intensity, i.e. all pixels in the k^{th} image were multiplied by the factor $\bar{I}_f / \bar{I}_f(k)$, where $\bar{I}_f$ is the overall mean forest intensity obtained by averaging these values. The

variation of $\bar{I}_f(k)$ over each of the FBD footprints was slightly different but use of this localised information should improve detection rate of changes due to deforestation which are comparable in size to the variation of $\bar{I}_f(k)$ (Whittle et al. 2011). The temporal standard deviation for a pixel at position **x** with intensity $I(\mathbf{x},t_i)$ sampled at times t_i, i = 1-N is defined as

$$SD(\mathbf{x}) = \left[\frac{1}{N-1} \sum_{i=1}^{N} \left(I(\mathbf{x},t_i) - \mu(\mathbf{x}) \right)^2 \right]^{\frac{1}{2}} \qquad (3)$$

where $\mu(\mathbf{x}) = \frac{1}{N} \sum_{i=1}^{N} I(\mathbf{x},t_i)$ is the temporal mean. Values of *SD* were obtained from the appropriate set of 12 forest-normalised ScanSAR images, excised over the FBD footprint and re-sampled to the FBD pixel size 12.5m. Treated in this way the ScanSAR data could deliver detection levels at P_{fa}= 0.2 almost as good as those from the FBD comparisons (see section 4). The FBD and multi-temporal data are derived from different sources and contain significantly different information. Consequently, we found that improved detection levels could be obtained using these data in combination.

3.4 Texture measures of change

We have chosen two texture measures for this study(Oliver and Quegan 2004), the first is the ratio of local spatial variance and mean of the intensity $I(\mathbf{x})$ at position **x**

$$tex1(\mathbf{x}) = \left\langle I(\mathbf{x})^2 \right\rangle \Big/ \left\langle I(\mathbf{x}) \right\rangle^2 - 1 \qquad (4)$$

where the angular brackets denote averages over a small window of length *wl* pixels. The second is a normalised log measure

$$tex2(\mathbf{x}) = \log\left\langle I(\mathbf{x}) \right\rangle - \left\langle \log\left[I(\mathbf{x}) \right] \right\rangle , \qquad (5)$$

which should be a more optimal measure for multi-look images(Oliver 1993). For the intensities we found that the standard ratios $R(\mathbf{x}) = I_{old}(\mathbf{x}) / I_{new}(\mathbf{x})$ detected deforestation through either increase or decrease of the intensity in either channel, resulting in four possible measures. Combination of the increases and the decreases lead to the use of $R_1(\mathbf{x})$ eq. (1) and further combination of the resulting HH and HV terms led to $R1$ eq. (2). Each stage of combination led to an increase in the detection rate of deforestation because of the differences between the regions detected by the individual measures. The texture measures also generate increases and decreases for both polarizations.

3.5 Comparison of measures

A convenient measure of the degree of overlap between two classes is the Simpson coefficient (Holliday et al. 2003); for two classes containing k and l pixels whose overlap contains m pixels, this is given by:

$$S_{sim} = \frac{m}{\min(k,l)}. \tag{6}$$

This expresses the overlap as a fraction of the smallest class; complete overlap of either class by the other yields a value of unity. Tables analyzing the overlap between components as measured by the Simpson coefficient are given below for the 10% acceptance level.

In each case the first table shows the degree of overlap with DF (the deforestation regions) and UF (the undisturbed forest regions remaining in the nf08 database).

Table 3. Simpson coefficients representing the degree of overlap between pixels at the 10% level for each measure with the deforested regions (DF) and the undisturbed regions (UF). For scene P443-F7170.

	Region	***HH***		***HV***			
		Increase	Decrease	Increase	Decrease	Row-sum	Rs
Intensity	DF	0.8344	0.6643	0.6822	0.9614	3.1423	3.664
	UF	0.1656	0.3357	0.3178	0.0386	0.8577	
***tex*1**	DF	0.6123	0.6391	0.6812	0.8235	2.7561	2.216
	UF	0.3877	0.3609	0.3188	0.1765	1.2439	
***tex*2**	DF	0.6528	0.7429	0.6996	0.8576	2.9529	2.820
	NF	0.3472	0.2571	0.3004	0.1424	1.0471	

The three sets of results are broadly similar – each measure shows a higher degree of correlation with deforested regions than with undisturbed regions, which is why they can be used for detection. In each case the penultimate column gives the row-sum of Simpson coefficients for the 4 terms and Rs gives the ratio of these for deforested compared with undisturbed regions. These ratios rank in the order Intensity > Texture 2 > Texture 1, which reflect the overall detection performance of these measures at this threshold.

The degree of cross-correlation between pixels associated with the four intensity changes, HH-increase, HH-decrease, HV-increase and HV-decrease, is reported as the Simpson coefficient in Table 4. The highest value in the table is 0.32; hence, although there is some overlap between the four types of detection, they are significantly different, even when they have the same sign. The values in the leading diagonals are notably larger than the off-diagonal terms, showing that changes of the same sign in HH and HV are more closely associated than changes of opposite sign; The tables for changes in *tex*1 and *tex*2 show a very similar pattern suggesting that, like the intensity, the texture measures show a significant degree of difference between the four components, which justifies the use of a similar combination strategy.

Table 4 Simpson coefficients representing the degree of overlap between pixels at the 10% level for increases and decreases in each measure. For scene P443-F7170.

(a) Intensity		***HH***	
		Increase	Decrease
HV	Increase	0.2706	0.0129
	Decrease	0.0716	0.3206

(b) Tex1		*HH*	
		Increase	Decrease
HV	Increase	0.3784	0.0252
	Decrease	0.0222	0.3162

(c) Tex2		*HH*	
		Increase	Decrease
HV	Increase	0.4196	0.0205
	Decrease	0.0172	0.3772

Tables 5a-c show the degree of cross-correlation between the measures, again from the Simpson overlap. There are no values in table 5a or 5b above 0.31 showing that there are also differences between the intensity and either texture measure which might be exploited by combination. In comparison, values in the leading diagonal of Table 5c are relatively high indicating that there is significant correlation between the texture measures and consequently that combination of these may be less fruitful.

Table5a. Simpson coefficients representing the degree of overlap between pixels at the 10% level for increases and decreases in intensity and *tex*1.

(a)			***Intensity***			
			HH		**HV**	
			Increase	Decrease	Increase	Decrease
***tex*1**	**HH**	Increase	0.2777	0.0705	0.0953	0.1461
		Decrease	0.0899	0.1677	0.1477	0.1463
	HV	Increase	0.1819	0.1437	0.0854	0.2543
		Decrease	0.1301	0.1073	0.195	0.1642

Table 5b Simpson coefficients representing the degree of overlap between pixels at the 10% level for increases and decreases in intensity and *tex*2.

(b)			***Intensity***			
			HH		**HV**	
			Increase	Decrease	Increase	Decrease
***tex*2**	**HH**	Increase	0.3103	0.0642	0.0983	0.1445
		Decrease	0.0968	0.1777	0.1538	0.1892
	HV	Increase	0.1995	0.1336	0.088	0.2318
		Decrease	0.1317	0.1182	0.1848	0.1889

Table 5c Simpson coefficients representing the degree of overlap between pixels at the 10% level for increases and decreases in texture1 and texture 2.

(c)			***tex1***			
			HH		**HV**	
			Increase	Decrease	Increase	Decrease
tex2	**HH**	Increase	0.8168	0	0.3874	0.018
		Decrease	0	0.7569	0.0256	0.3506
	HV	Increase	0.3872	0.0198	0.8215	0
		Decrease	0.0191	0.3164	0	0.8398

In the light of the above discussion, the raw texture measures for image pairs were then treated in the same way as intensities, Eq. (1), to obtain modified ratios

$$Q(\mathbf{x}) = \max\left[\frac{T_{old}(\mathbf{x})}{T_{new}(\mathbf{x})}, \frac{T_{new}(\mathbf{x})}{T_{old}(\mathbf{x})}\right] - 1 \ , \qquad (7)$$

for each location **x**, where T is a textural measure, either *tex*1 or *tex*2. These were obtained for both polarizations, *HH* and *HV*, which, following the treatment of intensities above, can be combined to give a change measure for each of the textural measures,

$$T1 = \tfrac{1}{2}\left[Q^{tex1}(HH) + Q^{tex1}(HV)\right] \ ; \qquad T2 = \tfrac{1}{2}\left[Q^{tex2}(HH) + Q^{tex2}(HV)\right] \qquad (8)$$

Experiments using different window lengths are detailed in the Appendix from which we concluded that, as found for the intensities(Whittle et al. 2011), a window of side *wl*=23 was optimal.

3.6 Combination techniques

The measures *SD*, *R*1, *T*1 and *T*2 have different ranges, but they can each be mapped to a value between 0 and 1 by the transformation

$$\hat{A}(\mathbf{x}) = \frac{A(\mathbf{x}) - A_{\min}}{A_{\max} - A_{\min}} \qquad (9)$$

where $A_{\max}$ and $A_{\min}$ are the maximum and minimum values of the measure A over the region. The transformed values can then be combined using techniques of data fusion (Whittle et al. 2004). The basic method simply adds the transformed quantites together giving the new measure *sums* defined by:

$$sums(\mathbf{x}) = \hat{A}(\mathbf{x}) + \hat{B}(\mathbf{x}) + \hat{C}(\mathbf{x}) + ... \qquad (10)$$

where $\hat{B}(\mathbf{x})$, $\hat{C}(\mathbf{x})$ are the transformed values of other measures. Other data fusion schemes were considered, but in general we found that the sum-rule gave the best results and is the only data fusion measure reported here. For brevity, we will notate a combination such as that in Eq. (4) as: *sums*-A-B-C.

Principle component analysis(Jolliffe 2002) (PCA) transforms multivariate data to a new space of orthogonal variables in which the first principle component is the linear sum of the original variables having maximal variance. These were computed using the MATLAB routine *princomp* using standardised variables (centred and scaled by the standard deviation). The results of this procedure were then rescaled to 0-1 to avoid negative values. We report here values based only on the first principle component for each combination, which we label as PCA1. Thus a PCA combination of the three measures A, B, and C will be notated as PCA1-A-B-C.

4. Results

4.1. Inclusion of texture

We start by examining results for the scene used in the original study: P443_F7170. Using the FBD data, the intensity and both texture measures have been used to obtain the measures *R*1, *T*1 and *T*2 as shown in sections 3.2 and 3.4. From these and their combinations ROC curves were then prepared by comparison of the detections at a series of threshold values with the known deforestation according to the databases (see section 3.1). As anticipated from the results of Table 3, the detection rate for the single measures is in the order *R1>T2>T1*. Combination of either texture measure with R1 using the range-scaled summation technique (Section 3.6) improves the detection performance, but a combination of all three measures cannot improve on the result for the 2-way combination *sums*-R1-T2. There is always a trade-off between false alarm and detection but these figures indicate that the main region of practical use lies between 0.1 and 0.2, where the curves deviate most from a diagonal line ((0,0) to (1,1)) that could be achieved by randomly choosing pixels. However, combination using *sums* gives a clear advantage over this range (see Fig. 2(b)) with the best result obtained by combining *R1* and *T2*; the further inclusion of *T*1 gives no advantage and is slightly detrimental. Notably at very low P_{fa} (<0.02) there is nothing to be gained by combination, the intensity measure *R*1 alone is as good as any.

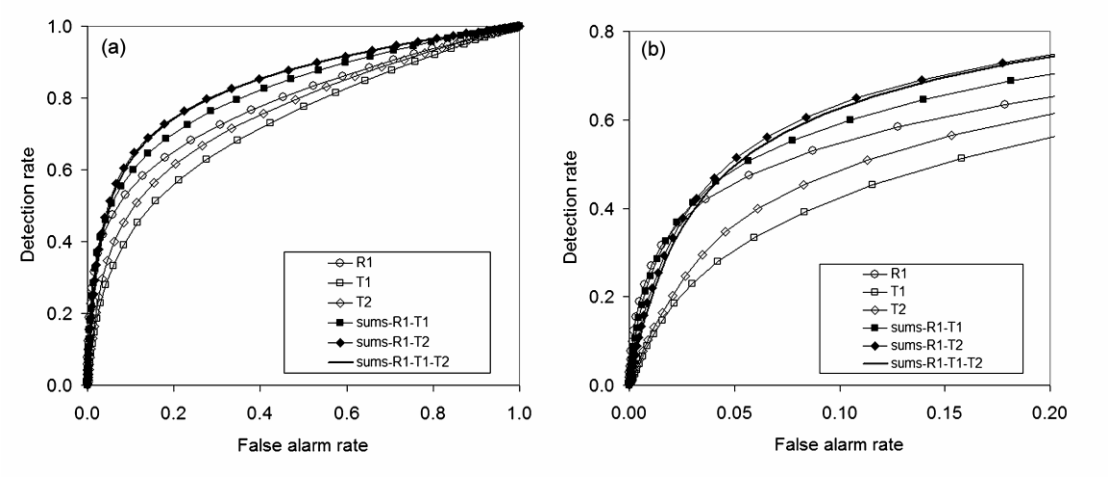

Figure 2 . ROC curves for the FBD scene P443_F7170, comparing detection rates obtained using (from the top of the legend); *R*1: the modified intensity ratios (eq. (2)), *T1*, *T2* modified ratios obtained using the textural measure tex1 and tex2 respectively; sums-*R1-T1* sum-fusion of *R1* and *T1*; sums-*R1-T2* sum-fusion of *R1* and *T2*; *sums-R1-T1-T2*: 3-way range-scaled sum fusion of *R1*, *T1*, *T2*. For: (a) full range; (b) detail at low P_{fa}.

In the original study we combined *R*1 with multi-temporal ScanSAR results, *SD*, and obtained enhancements of ~10% over *R1* alone. Further combinations including the textural measure T2 are shown in figure 3. The best combination over the range P_{fa} = 0.1-0.2 is the principle component combination of *R1*, *T2* and *SD* which narrowly exceeds the *sums* combination of the same components at P_{fa} = 0.1 and 0.2. Again the inclusion of *T1* in the combination is detrimental. It is again clear that for very small Pfa (<0.02) the FBD *R1* measure alone cannot be improved on.

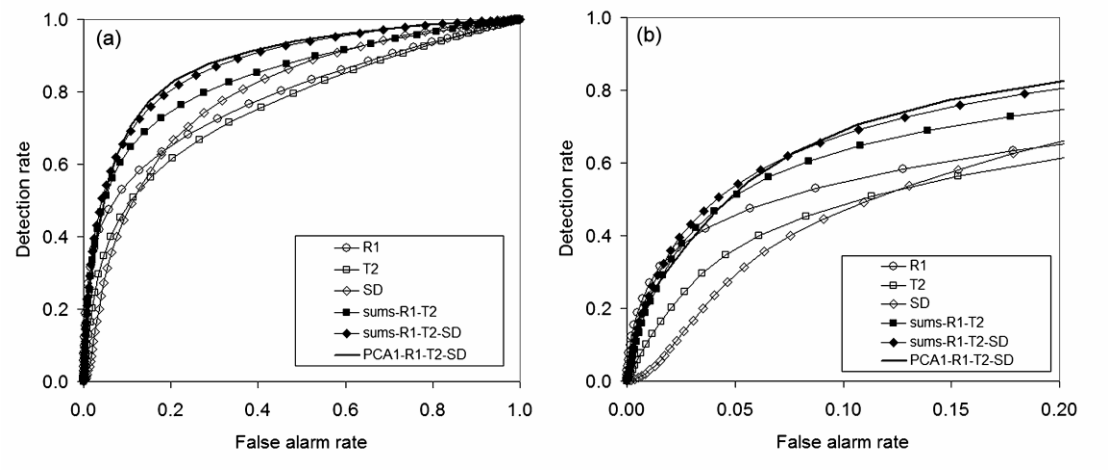

Figure 3. ROC curves for the FBD scene P443_F7170, comparing detection rates obtained by including texture T2 and ScanSAR *SD*. using (from the top of the legend); *R1*: the modified intensity ratios (eq. (2)), *T2* : modified ratios obtained using the textural measure tex2; SD: ScanSAR temporal standard deviation; sums-*R1-T2* sum-fusion of *R1* and *T2*; sums-*R1-T2-SD* sum-fusion of *R1*, *T2* and *SD*; PCA1-*R1-T2-SD*: first principle component combination of *R1*, *T2*, *SD*. For (a) full range; (b) detail for low P_{fa}.

Detection maps for the individual measures and the best combination method are compared with the database map of deforestation in figure 4. The similarity between the maps obtained using *T1* and *T2* (Figure 4(c) and (d)) are clear, as is the difference between these maps and that obtained using intensity, figure 4(a). The oblong feature right of centre, labelled "A" on the database map figure 4(f), stands out clearly as a region of low HV scattering in an RGB image of the scene (see supplementary information)(Whittle et al. 2011), is clearly picked out by *R*1 and ScanSAR SD but only the boundaries show using the texture measures (Fig. 4(c) and (d)). However, the nearby anvil-shaped triangular region of deforestation, labelled "B" in figure 4(f), shows as a weak feature in the RGB image, is hardly visible using *R*1, but is picked out by the texture measures and by the ScanSAR results Figure 4(b). In combination these detections reinforce each other to show the feature quite clearly at the 20% threshold level in figure 4(e). The ScanSAR result, figure 4(b) is relatively clear of salt-and-pepper type noise and it seems that the combined result 4(e) benefits from this in comparison to the single measures R1, T1 and T2.

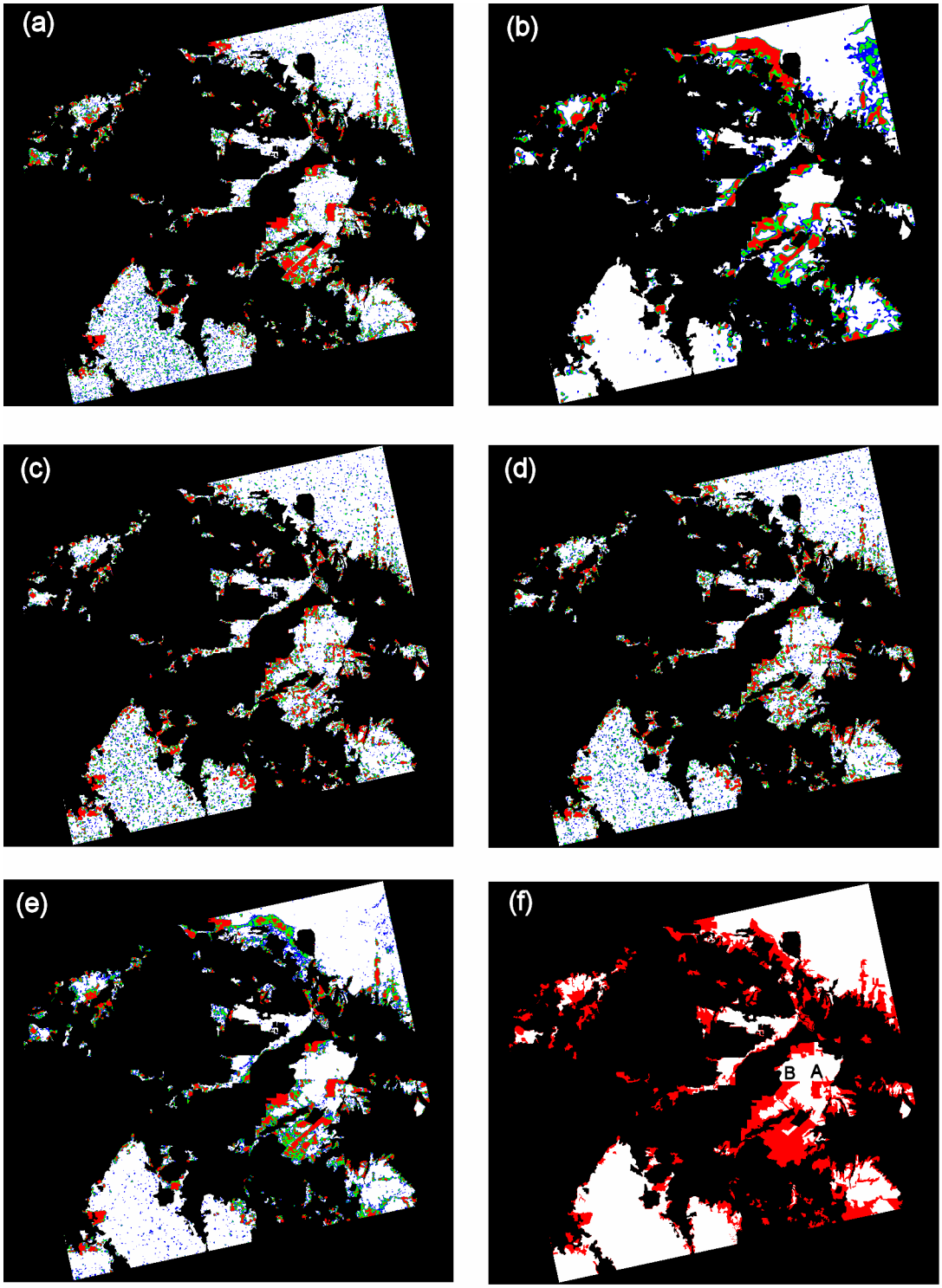

Figure 4. Detection maps for the FBD scene P443_F7170. In each case the white background represents the extent of natural forest in 2007 overlaid with detections at the, (red) 10%, (green) 20% and (blue) 30% acceptance thresholds. (a) *R1*; (b) *SD*; (c) *T1*; (d) *T2*; (e) the best combination result PCA1-*R1*:*T2*:*SD*; (f) showing the database estimate of deforestation during 2007-8 in red. The labelled regions "A" and "B" are referred to in the text.

4.2 Transferability

The scene P443-F7190 (Figure 1(c)) shows part of the Kampar peninsular, a region that includes a peat dome(Hooijer et al. 2010; Pearce 2007) some 15m deep. It appears as a darker patch on the RGB image (see supplementary information) indicating a lower level of backscatter in both channels. Detection maps for the individual measures and the best combination method are compared with the database map of deforestation in figure 5. The vicinity of the peat dome region appears in the ScanSAR multi-temporal result Figure 5(b) as a large white patch left of centre, indicating a scarcity of detections and a relatively stable region. In contrast, some significant changes in this area are shown using *R1* in figure 5(a), which in fact appear in both the HH and HV components of *R*1. The two textural measures (figure 5c, d) again show very similar pattern of detection to each other but fail to distinguish the peat dome from the surrounding forest. The best detection probability for deforestation in this case is achieved by the sum-rule fusion of all four measures, *sums-R*1-*T*1-*T*2-*SD*, which exceeds the principle component combination of the same set by 4% at P_{fa} = 0.2. It also narrowly exceeds the PCA combination of *R1*, *T2* and *SD* (the best combination for P443-F7170) by 1% at Pfa = 0.2.

Detection rates at Pfa = 0.1 and 0.2 for all measures and their combinations are compared in figure 6 for the four scenes. These figures reveal that the ScanSAR temporal standard deviation is not in general as good as R1 and also that there is a good deal of variation between the behaviour for the different scenes. They also show that T2 is always slightly better than T1, and that in one case, P443-F7190 – (Figure 6(b)) , both texture measures give a better retrieval performance than R1 alone. T2 (but not T1) improves on R1 for P445-F7170 (Figure 6(d)). Detection rates for P445-F7170 are uniformly lower than for other scenes (Figure 6(d)), and this is possibly because they are compromised by the significantly mountainous terrain of this scene. Working on boreal forests, Thiel et al. (Thiel et al. 2006), have noted that topography can increase the spread of SAR backscatter making it more difficult to discriminate between forest and non-forest areas. The performance of ScanSAR SD for this scene is particularly poor.

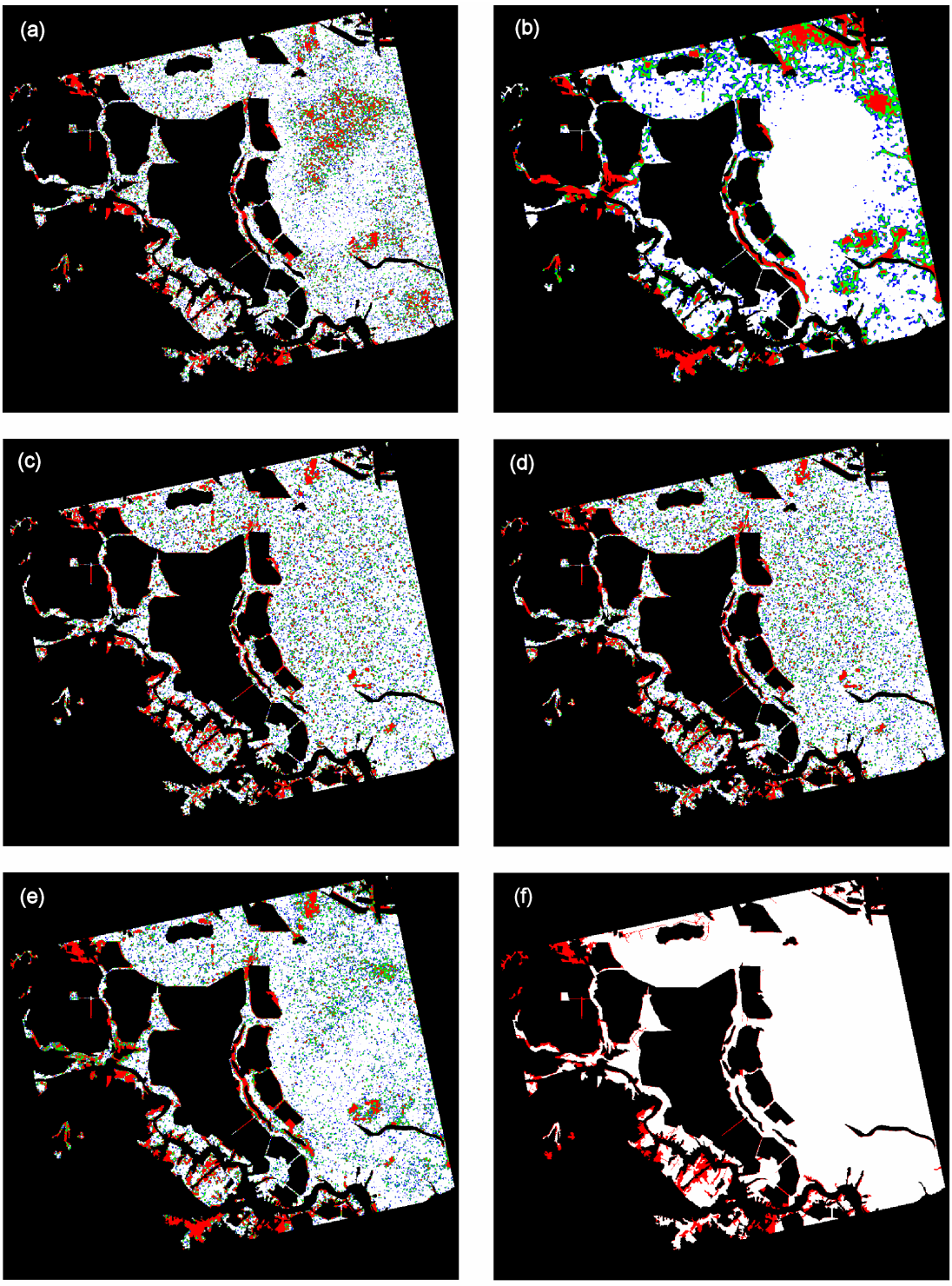

Figure 5 In each case the white background represents the extent of natural forest in 2007 overlaid with detections at the, (red) 10%, green 20% and blue 30% acceptance thresholds. (a) *R1*av; (b) *SD*; (c) *T1*; (d) *T2*; (e) the best combination result *R1*:*T1*:*T2*:*SD*-sums; (f) showing the database estimate of deforestation during 2007-8 in red.

In order to compare the consistency of change-measure performance between the different scenes, we take the detection rate obtained using *R*1 as an internal standard and consider other change measures in relation to it. We define the degree of detection enhancement, *E*, for a measure *M* over the basic result for *R*1 as,

$$E = \left[P_d(M) - P_d(R1)\right] / P_d(R1) \qquad (11)$$

where $P_d(M)$ refers to the detection rate for measure *M*. and both detection rates are measured at the same P_{fa}. The enhancement values are plotted at P_{fa} = 0.1 and 0.2 for each scene in Figure 7. These plots show that combination is clearly a successful strategy for P443-F7190, Fig. 7(c), but is less so for the geographically adjacent P443-F7180 Fig. 7(b). The detection rate obtained using *R*1 alone, Fig 6(b), was relatively high for P443-F7180 and it could be that there is less room for improvement. They also show that in general the ScanSAR multi-temporal technique is almost as good as the FBD ratio method at P_{fa} = 0.2 except for P445_F7170, again probably due to the mountainous terrain for this scene. ScanSAR SD is generally less effective than *R*1 at low P_{fa}. Fig. 7(d) also shows that the relatively poor detection rate for ScanSAR *SD* suppresses most combinations that include it, the exceptions being those that were performed by PCA. Relatively poor performance by *SD* is also found in P443-F7180, Fig. 7(b), and similarly tends to suppress combination by all sum-rule combinations that include it. Combinations using PCA however, again give positive enhancement. A comparison of figures 7(b) and (d) thus show a similar pattern for the results at P_{fa} = 0.1. A comparison of all plots in Figure 7 further shows that the combination of *R*1 with texture measure *T*2 enhances all results and is in all cases better than a combination with *T*1. It is also better than PCA combinations that include *SD* when the *SD* retrieval is poor i.e. P443-F7180 and P445_F7170 figures 7(b) and (d). In fact, for P445_F7170, the inclusion of *SD* with *R*1 and *T*2 either by *sums* fusion or by PCA reduces the detection performance of the combination measure using only R1 and T2.

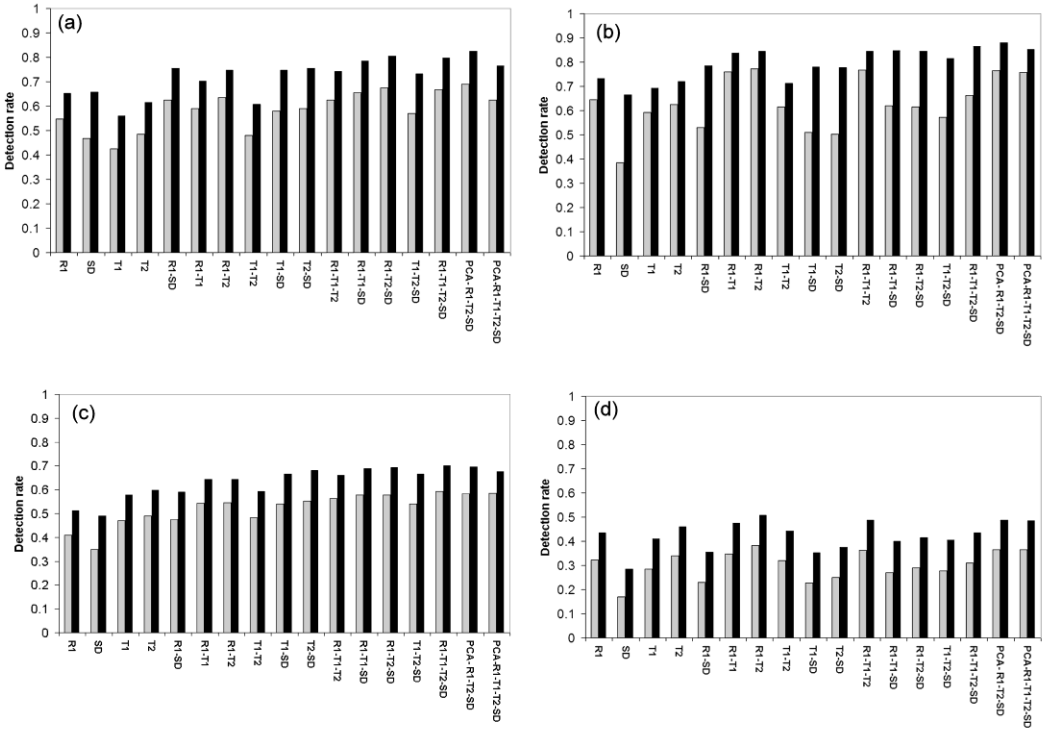

Figure 6. Comparison of detection rates for single detection measures and for combinations: ■ at Pfa = 0.1; ■ at Pfa = 0.2. (a) P443-F7170; (b) P443-F7180; (c) P443-F7190; (d) P445-F7170.

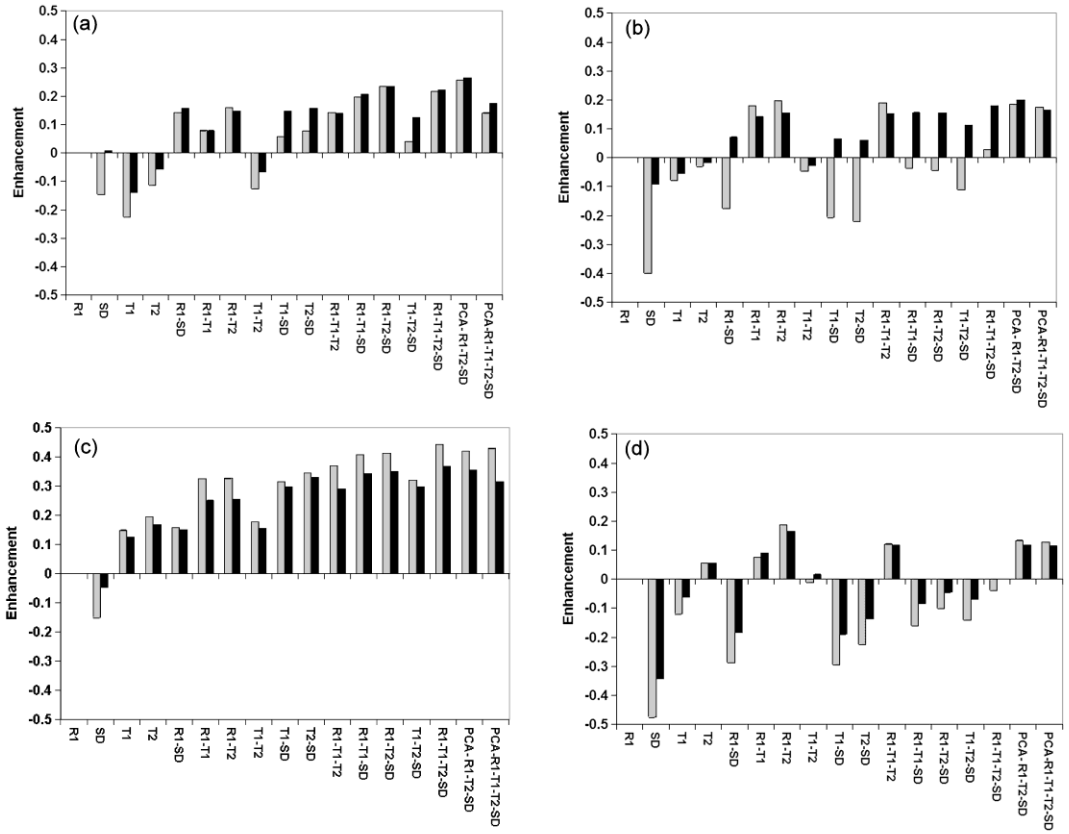

Figure 7. Comparison of detection enhancement compared with *R*1 for single measures and combinations as shown on the abscissa. : ■ at $P_{fa} = 0.1$; ■ at $P_{fa} = 0.2$. (a) P443-F7170; (b) P443-F7180; (c) P443-F7190; (d) P445-F7170.

The best detection rates obtained for each scene are summarised in Tables 6(a) and (b) for $P_{fa} = 0.1$ and 0.2. There is no consistent overall winner; however it is clear from the enhancement plots in Figure 7 that the combination of *R*1 and *T*2 with or without *SD* is, consistently useful. The inclusion of *T*1 rarely gives any extra improvement, thus the combination of all four measures is not usually optimal but does perform best for P443-F7190 (the 4-way sum-rule combination improves on *sums*-R1-T2-SD by 5.4%). There is no consensus in these tables about whether PCA or sums is the best. The inclusion of *SD* is positive 5 times out of 8 – however it is not helpful for the mountainous region (P445-F7170).

The fraction of forest that is deforested during 2007-8 is much less for scenes P443-F7180, P443-F7190 and P445-F7170 than for P443-F7170, which was the subject of the original study (Table 6). The threshold values give the percentage of natural forest in the nf07 database for each scene that was accessed to achieve the P_{fa} values given. Because we know the fraction of forest that is deforested between the nf07 and nf08 databases these values can be used to calculate the Precision, P_r, – the probability that a detected pixel is in a deforested region. The Precision is defined as

$$P_r = a/r \qquad (11)$$

Where r is the total number of pixels retrieved by detection and a is the number of detected pixels that are correctly assigned. The detection rate (sometimes called the Recall) is

$$P_d = a/k \tag{12}$$

where k is the total number of pixels that are actually part of the deforested region. We have defined the detection threshold T_h as the percentage of pixels that are retrieved from the whole region searched, which we suppose contains n pixels. Hence,

$$T_h = 100\, r/n \tag{13}$$

The Precision is then

$$P_r = 100\frac{P_d k}{T_h n} = 100\frac{P_d}{T_h} D_f \tag{14}$$

Where $D_f = k/n$ is the fraction of the searched region that is actually deforested. These values are given in the final column of Table 6 and the low values recorded for the new scenes reflect the difficulty of finding areas of deforestation when it makes up only a small proportion of the total area.

Table 6 also shows that the threshold value needed to achieve P_{fa} = 0.2, say, also depends on the proportion deforested. In use, these techniques would be applied to regions that have, by definition, an unknown proportion of deforestation, but the detection maps using threshold values 10%, 20% and 30% mostly cover the range of thresholds used in Table 6 to achieve P_{fa} values between 0.1 and 0.2.

Table6a Summary of best results by scene at P_{fa}=0.1

Scene	*DF-fraction*	*Threshold % total*	*Combination*	*Detection rate*	*Precision*
P443-F7170	0.301	27.7	PCA-*R1-T2-SD*	0.689	0.784
P443-F7180	0.090	16.0	*sums-R1*:*T2*	0.772	0.432
P443-F7190	0.058	12.8	*sums-R1*:*T1*:*T2*:*SD*	0.592	0.266
P445-F7170	0.081	12.3	*sums-R1*:*T2*	0.383	0.253

Table6b Summary of best results by scene at Pfa = 0.2.

Scene	*DF-fraction*	*Threshold % total*	*Combination*	*Detection rate*	*Precision*
P443-F7170	0.301	38.8	PCA-*R1-T2-SD*	0.824	0.639
P443-F7180	0.090	26.1	PCA-*R1-T2-SD*	0.879	0.302
P443-F7190	0.058	22.9	*sums-R1*:*T1*:*T2*:*SD*	0.702	0.177
P445-F7170	0.081	22.5	*sums-R1*:*T2*	0.508	0.183

The combinations that gave the best results at P_{fa}= 0.2 (Table 6b) have been used to compile the detection maps in Figure 8. Although quite a good visual comparison is evident between the detections for P443-F7180 and the database map, the river basins are clearly incorrectly highlighted. This error is mainly due to the introduction of ScanSAR data which, as we have noted, is known to be sensitive to flooding. Notably, the detection map, Fig. 9, obtained using *sums*-R1-T2, which was the best combination at P_{fa} = 0.1 (Table 6a), does not suffer from this error. At P_{fa} = 0.2 the inclusion of ScanSAR produced a marginal 3.3% improvement in detection rate over

sums-R1-T2. This suggests that in practice, if ScanSAR is available, a comparison of results with and without its use would be advised. However, in practice this sort of error would probably be spotted by those familiar with the region.

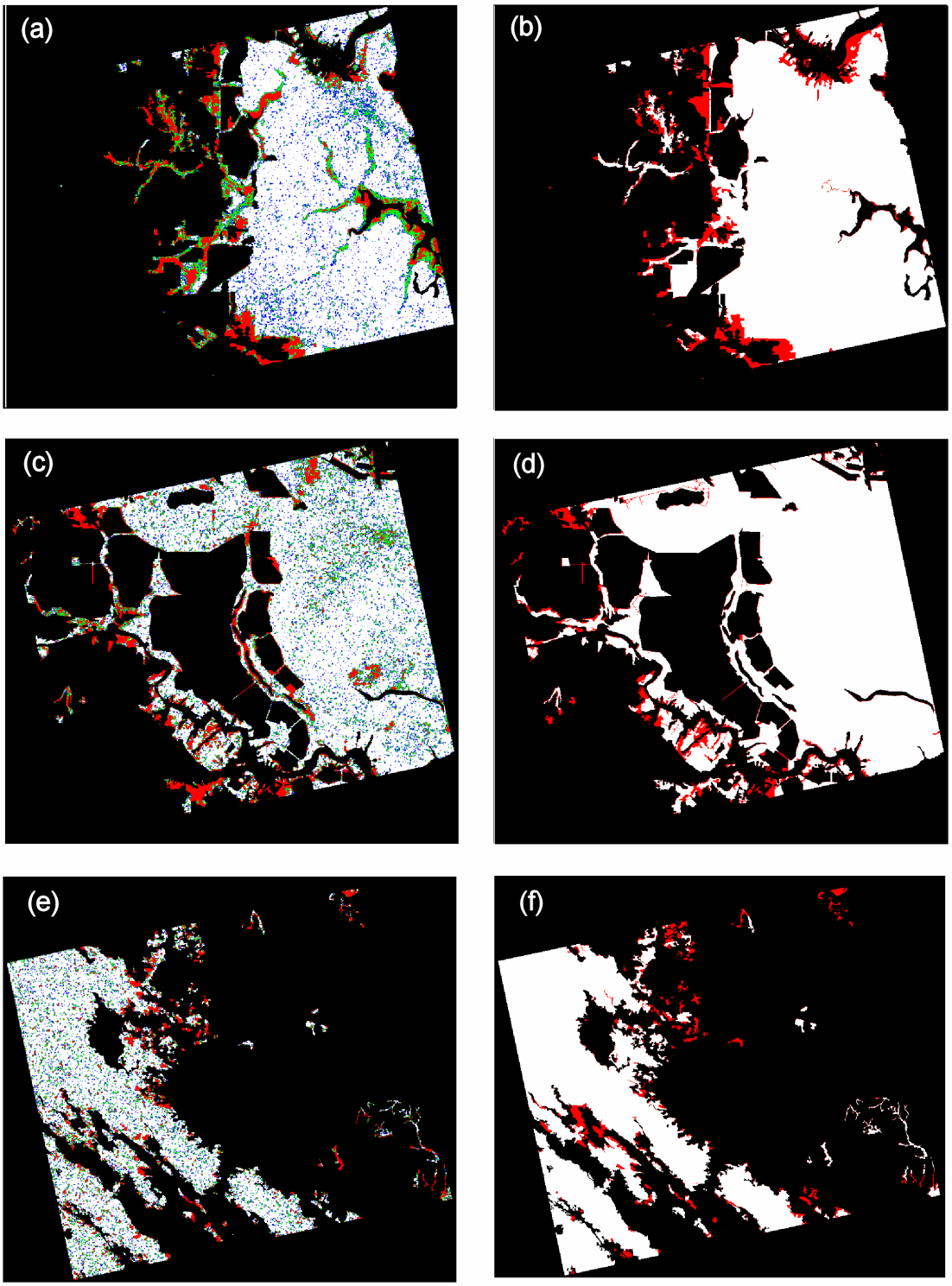

Figure 8 Compares the best combination results (table 6) with database-derived maps of deforestation. The detection maps are coloured: (red) 10%, green 20% and blue 30% acceptance thresholds on a white background representing the natural forest in 2007. The associated database maps show regions deforested during 2007-2008 in red. For (a) P443-F7180 (PCA-R1-T2-SD) and (b) database; (c) P443-F7190 (sums-R1-T1-T2-SD) and (d) database; (e) P445-F7170 (sums-R1-T2) and (f) database. Comparable results for F443-F7170 are shown in figure 4.

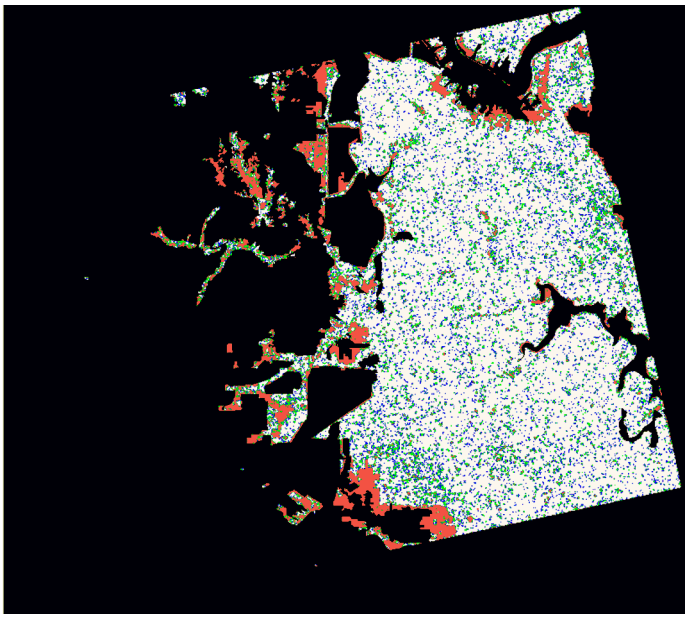

Figure 9. Detection map using the combination sums-R1-T2 for P443-F7180, with: (red) 10%, green 20% and blue 30% acceptance thresholds on a white background representing the natural forest in 2007.

Taking the average enhancement values over all of the scenes we obtain Fig. 10, which clearly shows that a principle component combination of *R*1, *T*2 and *SD* is the overall best choice of combination achieving an average of 24.9% and 23.4% enhancement at P_{fa} = 0.1 and 0.2 respectively. However, if the ScanSAR temporal standard deviation is not available, then the sum-rule combination of *R*1 and *T*2 (which achieve average enhancements of 21.7% and 18.0% at P_{fa} = 0.1 and 0.2) is clearly preferred over the combination of *R1* and *T1*. This suggests that, on the basis of our data, these are the best procedures to use in practice when searching for deforestation in a new region.

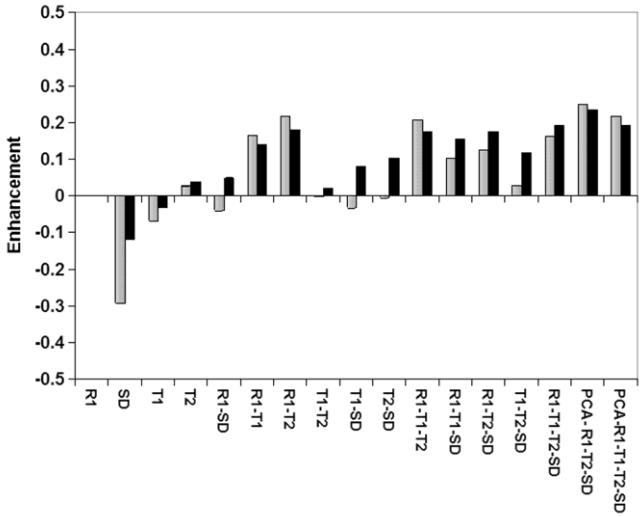

Figure 10. Plot of the average enhancement values over all four scenes: ■ at P_{fa} = 0.1; ■ at P_{fa} = 0.2.

In the absence of any prior knowledge about the areas deforested it is not possible to obtain results at a standard value of P_{fa}; this is only useful for the analysis. In practice results must be obtained at some given threshold level. In the light of our conclusions based on a consideration of the average enhancement Fig. 10, Tables 7 a-d give the equivalent P_{fa}, P_d and P_r values for each of the scenes considered here, using the PCA combination of *R1*, *T2*, *SD* for the three values of threshold used in developing the detection maps. The equivalent values for the sum-fusion of *R*1 and *T*2 are also shown. They show that the P_{fa} varies considerably at the 20% threshold (green in the maps) for the 4 scenes but is always below the 0.2 level used as a standard here. As expected, while values of the detection rate increase with increasing threshold, the precision falls. At the 20% threshold the 3-way combination produces a slightly better detection rate only for P443_F7180 and P443_F7190.

Table 7

P443_F7170

PCA1-R1-T2-SD				*sums-R1-T2*		
T_h	P_{fa}	P_d	P_r	P_{fa}	P_d	P_r
10%	0.017	0.286	0.859	0.017	0.292	0.879
20%	0.053	0.532	0.799	0.056	0.533	0.801
30%	0.114	0.72	0.721	0.132	0.682	0.683

P443_F7180

PCA1-R1-T2-SD				*sums-R1-T2*		
T_h	P_{fa}	P_d	P_r	P_{fa}	P_d	P_r
10%	0.051	0.592	0.532	0.042	0.667	0.598
20%	0.136	0.827	0.371	0.139	0.808	0.363
30%	0.239	0.899	0.269	0.241	0.865	0.259

P443_F7190

PCA1-R1-T2-SD				*sums-R1-T2*		
T_h	P_{fa}	P_d	P_r	P_{fa}	P_d	P_r
10%	0.072	0.529	0.305	0.073	0.505	0.291
20%	0.166	0.664	0.191	0.17	0.619	0.178
30%	0.269	0.743	0.143	0.27	0.693	0.133

P445_F7170

PCA1-R1-T2-SD				*sums-R1-T2*		
T_h	P_{fa}	P_d	P_r	P_{fa}	P_d	P_r
10%	0.077	0.329	0.267	0.078	0.345	0.281
20%	0.173	0.459	0.187	0.171	0.476	0.194
30%	0.27	0.553	0.15	0.272	0.577	0.156

5. Conclusions

We have found that, like the intensity, the textural measures *tex*1 and *tex*2 increase or decrease in response to deforestation and can be used as indicators of change. Paralleling our treatment of intensities, they have been combined to give the modified ratio measures *T*1 and *T*2; of these *T*2 has invariably given the better results alone or in combination. We have examined results over 4 scenes and on their own these measures succeed in detecting deforestation in some cases less and in some more than the equivalent intensity measure *R*1. The key point however is that they contain different information to the intensity-based measure so that when used in combination with *R*1 the detection rate of deforested regions is improved. When combined with *R*1 using data-fusion summation the modified ratio *T*2 gave an average enhancement of 18.0% at P_{fa} = 0.2 over the four scenes (Figure 10). The equivalent value for *T*1 was 14.0%. Since *T*1 and *T*2 are quite strongly correlated (Table 5c) we have not generally found it useful to use both measures in combination. In the earlier work we also achieved enhanced detection of deforested areas by combining *R*1 with temporal standard deviation *SD* derived from ScanSAR images. In this work we have achieved an enhancement of 15.6% in detection rate at P_{fa} = 0.2 using *sums-R*1-*SD* for the scene P443-F7170. However, the equivalent average result (see Figure 10) for this combination is dragged down to just 4.5% by the inclusion of poor performance by

ScanSAR *SD* in other scenes, particularly P445-F7170. Nevertheless, even including this result, the principle component combination of *R*1, *T*2 and *SD* gave the best overall enhancement of 23.4% at P_{fa} = 0.2. The principle component combination of these measures was a significant improvement over the data fusion summation technique: the average enhancement for *sums*-R1-T2-SD was 17.3% at P_{fa} = 0.2, less than the 18% enhancement obtained for *sums*-R1-T2. The values obtained using these combinations for the individual scenes is summarised in Table 8. There was considerable variation between the results obtained and, as we have already noted, the inclusion of ScanSAR *SD* for P445-F7170 is detrimental to the combination of *R*1 and *T*2 alone.

Table 8. Summary of best results obtained for the four FBD scenes.

	sums-R1-T2		*sums-R1-T2-SD*		*PCA1-R1-T2-SD*	
Scene	P_{fa}=0.1	P_{fa}=0.2	P_{fa}=0.1	P_{fa}=0.2	P_{fa}=0.1	P_{fa}=0.2
P443-F7170	0.635	0.747	0.676	0.805	0.689	0.824
P443-F7180	0.772	0.846	0.616	0.846	0.764	0.879
P443-F7190	0.544	0.644	0.579	0.693	0.582	0.695
P445-F7170	0.383	0.508	0.290	0.416	0.366	0.487

We have thus shown that the enhancements available by the inclusion of texture into a detection algorithm are worthwhile. The procedure we have described requires only FBD images, is straightforward and quick and provides a simple extension to an analysis using intensities alone. The further inclusion of multi-temporal ScanSAR *SD* involves laborious co-registration, excising the FBD footprint region from the results and re-sampling to the FBD pixel size. Our results show that it should not be used in combination with the FBD results over mountainous terrain, although it may be that compensation using a digital elevation model (DEM) could improve matters(Santoro et al. 2009). This is not possible with the level 1.5 processed data and GAMMA software that we have used here. The procedure would require level 1.1 single-look complex data (SLC) data, however this would add an extra layer of complexity to the analysis and it must be questioned whether it is worthwhile in relation to the enhancements that can be obtained. A more reasonable approach for monitoring would be to use ScanSAR multi-temporal method as a preliminary screen followed by the use of FBD with combined intensity and texture measures. In practice, as a monitoring tool, the only accessible variable is the threshold value T_h, and, through a choice of threshold values, the detection maps. Table 7 shows that for a 20% threshold the inclusion of ScanSAR results only improves enhancement of the detection rate and precision for two of the available scenes. Furthermore, the precision values, which give the probability that a detected pixel correctly identifies a deforested region, are shown to be very low if the fraction of forest affected by deforestation is low. In this sense the methods described here are best thought of as screening tools used to narrow a search before choosing areas that should go forward for optical confirmation or ground-based scrutiny.

The focus of this paper has been on the inclusion of textural measures. However, this work has used corrected versions of the original databases and it is notable that this has produced slight improvements in the detection rates obtained. These are summarised in Table 9

Table 9. Comparison of values obtained for P_d at P_{fa} = 0.2 from the original study with the results of this work using the updated databases.

Change measure	*Original databases*	*Updated databases*	*Change*
*R*1	0.635	0.652	+0.017
SD	0.613	0.657	+0.044
*sums-R*1*-SD*	0.718	0.754	+0.036

These improvements in detection are in line with the expectations of the error analysis given in that paper. However, it is worth noting that some of the sources of error remain and that the estimates of detection rates given here may still underestimate the true values.

Acknowledgements

This work was carried out with the support of the ALOS Kyoto & Carbon Initiative, (http://www.eorc.jaxa.jp/ALOS/en/kyoto/kyoto_index.htm) which is an international initiative led by the JAXA Earth Observation Research Centre (EORC), set up to support data and information needs raised by international environmental conventions, carbon cycle science and conservation of the environment. We thank Yumiko Uryu and Koko Yulianto from WWF for continued support and access to the databases used. We also thank Sue Page, Kevin Tansey and Matt Waldram from the Dept of Geography at Leicester University for helpful discussions. MW thanks Maurizio Santoro of Gamma Remote Sensing for helpful advice.

Appendix

Dependence of textural measures on window length

We have previously determined that a window length of 23 is optimum for window-averaged intensity ratios(Whittle et al. 2011). It is not obvious that the same length should also apply to the textural measures either individually or in combination so Table A1 compares detection rate, P_d, values for *T*1 for false alarm rate, P_{fa}, =0.2 on the ROC curve for textures obtained at several window lengths.

Table A1a. Detection rates at P_{fa}=0.2 obtained from ROC curves for FBD image P443_F7170 as a function of window length (*wl*) for *tex*1 and tex2 values. Combinations are made with *R*1 prepared using a window length of 23. The comparable detection rates for *R*1 and *SD* alone are 0.635 and 0.613 respectively. The final column, PCA1, refers to the first component of a principle component analysis using all four descriptors.

			Combination by *sums*					PCA1
wl	*T1*	*T2*	*R1*:*T1*	*R1*:*T2*	*R1*:*T1*: *SD*	*R1*:*T2*: *SD*	*R1*:*T1*: *T2*:*SD*	*R1*:*T1*: *T2*:*SD*
7	0.451	0.473	0.666	0.680	0.732	0.745	0.678	0.640
11	0.487	0.521	0.702	0.702	0.775	0.761	0.729	0.688
15	0.516	0.558	0.707	0.724	0.784	0.783	0.765	0.721
19	0.540	0.588	0.705	0.738	0.786	0.797	0.785	0.746
23	0.561	0.614	0.703	0.747	0.786	0.805	0.797	0.765

Table A1b. Detection rates at Pfa =0.1 obtained from ROC curves for FBD image P443_F7170 window length, *wl* = 23 for *tex*1 and tex2 values. The comparable detection rates (at Pfa =0.1) for *R1* and *SD* are 0.527 and 0.419 respectively.

			Combination by *sums*					PCA1
wl	*T1*	*T2*	*R1*:*T1*	*R1*:*T2*	*R1*:*T1*: *SD*	*R1*:*T2*: *SD*	*R1*:*T1*: *T2*:*SD*	*R1*:*T1*: *T2*:*SD*
23	0.424	0.485	0.591	0.635	0.656	0.676	0.667	0.625

Columns 2 and 3 of Table 1 show that retrieval using the textural measures increases with window size up to the maximum of 23. Detection rates for the combination with values of R1 (windowed at length 23) pass through a small maximum at wl=15 for tex1 while for tex2 they also increase up to the maximum window size. When the ScanSAR temporal standard deviation values, SD, are included in the combination (columns 6-9) results essentially reach a plateau for *T1* and increase up to the maximum window size when *T2* is included. Combination of all four descriptors either by range-scaled summation or using the first component of a principle component analysis (PCA1) does not improve on the 3-way range-scaled summation of *R1* ,*T2* and *SD* and the best result is obtained using a window size of 23 to prepare the textural measure. Table 1b shows that the same conclusion holds for results at a false alarm rate of 0.1 at *wl* = 23. The results given here were therefore prepared using textures obtained with *wl*=23.

References

Achard, F., Eva, H.D., Stibig, H.-J., Mayaux, P., Gallego, J., Richards, T., & Malingreau, J.-P. (2002). Determination of Deforestation Rates of the World's Humid Tropical Forests. *Science, 297*, 999-1002

Bonan, G.B. (2008). Forests and Climate Change: Forcings, Feedbacks, and the Climate Benefits of Forests. *Science, 320*, 1444-1449

Broich, M., Hansen, M.C., Stolle, F., Potapov, P.V., Arunarwati, B., & Adusel, B. (2011). Remotely sensed forest cover loss shows high spatial and temporal variation across Sumatera and Kalimantan, Indonesia 2000-2008 *Environmental Research Letters, 6*, 014010-014019

DeFries, R.S., Rudel, T., Uriarte, M., & Hansen, M.C. (2010). Deforestation driven by urban population growth and agricultural trade in the twenty-first century. *Nature Geoscience, 3*, 178-181

Fuller, D.O. (2006). Tropical forest monitoring and remote sensing: A new era of transparency in forest governance? *Singapore Journal of Tropical Geography, 27*, 15-29

Goetz, S.J., Baccini, A., Laporte, N.T., Johns, T., Walker, W., Kelindorfer, J., Houghton, R.A., & Sun, M. (2009). Mapping and monitoring carbon stocks with satellite observations: a comparison of methods. Available from: http://www.cbmjournal.com/content/4/1/2, [Accessed: 05/05/2009]

Hansen, M.C., Stehman, S.V., Potapov, P.V., Arunarwati, B., Stolle, F., & Pittman, K.W. (2009). Quantifying changes in the rates of forest clearing in Indonesia from 1990 to 2005 using remotely sensed data sets. *Environmental Research Letters, 4*, 034001

Hansen, M.C., Stehman, S.V., Potapov, P.V., Loveland, T.R., Townshend, J.R.G., DeFries, R.S., Pittman, K.W., Arunarwati, B., Stolle, F., Steininger, M.K., Carroll, M., & DiMiceli, C. (2008). Humid tropical forest clearing from 2000 to 2005 quantified by using multitemporal and multiresolution remotely sensed data. *Proceedings of the National Academy of Sciences of the United States of America, 105*, 9439–9444

Holliday, J.D., Salim, N., Whittle, M., & Willett, P. (2003). Analysis and Display of the Size Dependence of Chemical Similarity Coefficients. *Journal of Chemical Information and Computer Science, 43*, 819-828

Hooijer, A., Page, S.E., Canadell, J.G., Silvius, M., Kwadijk, J., Woosten, H., & Jauhiainen, J. (2010). Current and future CO_2 emissions from drained peatlands in Southeast Asia *Biogeosciences, 7*, 1505-1514

Houghton, R.A. (2005). Above ground Forest Biomass and the Global Carbon Balance. *Global Change Biology, 11*, 945-958

Houghton, R.A. (2010). How well do we know the flux of CO2 from land-use change? *Tellus, 62B*, 337-351

IPCC (2007). Climate Change 2007: The Physical Science Basis. Contribution of Working Group I to the Fourth Assessment Report of the Intergovernmental Panel on Climate Change In S. Solomon, D. Qin, M. Manning, Z. Chen, K.B. Marquis, Averyt, M. Tignor & H.L. Miller (Eds.): Cambridge University Press, Cambridge, United Kingdom & New York, NY, USA

Jolliffe, I.T. (2002). *Principal component analysis*. Berlin, London: Springer

Le Quéré, C. (2010). Trends in the land and ocean carbon uptake. *Current Opinion in Environmental Sustainability, 2*, 219-224
McAlpine, C.A., Ryan, J.G., Seabrook, L., Thomas, S., Dargusch, P.J., Syktus, J.I., Pielke, R.A., Etter, A.E., Fearnside, P.M., & Laurance, W.F. (2010). More than CO2: a broader paradigm for managing climate change and variability to avoid ecosystem collapse *Current Opinion in Environmental Sustainability, 2*, 334-346
Oliver, C., & Quegan, S. (2004). *Understanding Synthetic Aperture Radar Images*. Raleigh: SciTech
Oliver, C.J. (1993). Optimum texture estimators for SAR 1 clutter. *Journal of Physics D: Applied Physics, 26*, 1824-1835
Oliver, C.J. (2000). Rain Forest Classification Based on SAR Texture. *IEEE Transactions on Geoscience and Remote Sensing, 38*, 1095-1104
Page, S.E., Siegert, F., Rieley, J.O., Boehm, H.-D.V., Jaya, A., & Limin, S. (2002). The amount of carbon released from peat and forest fires in Indonesia during 1997. *Nature, 420*, 61-65
Pearce, F. (2007). Bog Barons: Indonesia's carbon catastrope. *New Scientist, 1 December*, 50-53
Pitman, A.J., Narisma, G.T., Pielke Sr., R.A., & Holbrook, N.J. (2004). Impact of land cover change on the climate of southwest Western Autstralia. *Journal of Geophysical Research, 109*
Quegan, S., & Yu, J.J. (2001). Filtering of Multichannel SAR images. *IEEE Transactions on Geoscience and Remote Sensing, 39*, 2373-2379
Raney, K.R. (1998). Chapter 2 - Radar Fundamentals: Technical Perspective. In R.A. Ryerson (Ed.), *Manual of remote sensing. Vol.2, Principles and applications of imaging radar / edited by Floyd M. Henderson and Anthony J. Lewis.* New York; Chichester: J. Wiley
Rignot, E.J.M., & van Zyl, J.J. (1993). Change detection techniques for ERS-1 SAR data. *IEEE Transactions on Geoscience and Remote Sensing, 31*, 896-906
Rosenqvist, A., Shimada, M., Ito, N., & Watanabe, M. (2007). ALOS PALSAR: A Pathfinder Mission fo Global-Scale Monitoring of the Environment. *IEEE Transactions on Geoscience and Remote Sensing, 45*, 3307-3316
Santoro, M., Fransson, J.E.S., Eriksson, L.E.B., Magnusson, M., Ulander, L.M.H., & Olsson, H. (2009). Signatures of ALOS PALSAR L-Band Backscatter in Swedish Forest. *IEEE Transactions on Geoscience and Remote Sensing, 47*, 4001-4019
Thiel, C., Drezet, P., Weise, C., Quegan, S., & Schmullius, C. (2006). Radar remote sensing for the delineation of forest cover maps and the detection of deforestation. *Forestry, 79*, 589-597
Uryu, Y., Purastuti, E., Laumonier, Y., Budiman, A., Yulianto, K., Sudibyo, A., Hadian, O., Kosasih, D.A., & Stüwe, M. (2010). Sumatra's Forests, their Wildlife and the Climate. Windows in Time: 1985, 1990, 2000 and 2009. . Available from: http://www.illegal-logging.info/item_single.php?it_id=1025&it=document, [Accessed: 08/02/2011]
Whittle, M., Gillett, V.J., Willett, P., Alex, A., & Loesel, J. (2004). Enhancing the Effectiveness of Virtual Screening by Fusing Nearest Neighbor Lists: A Comparison of Similarity Coefficients. *Journal of Chemical Information and Computer Science, 44*, 1840-1848
Whittle, M., Quegan, S., Uryu, Y., Stüewe, M., & Yulianto, K. (2011). Detection of tropical deforestation using ALOS-PALSAR. *Remote sensing of environment, Submitted*

Texture-enhanced detection of tropical deforestation using ALOS-PALSAR

MartinWhittle[a], Shaun Quegan[a], Yumiko Uryu[b] , Michael Stüewe[b], Koko Yulianto[c]

Supplementary Information

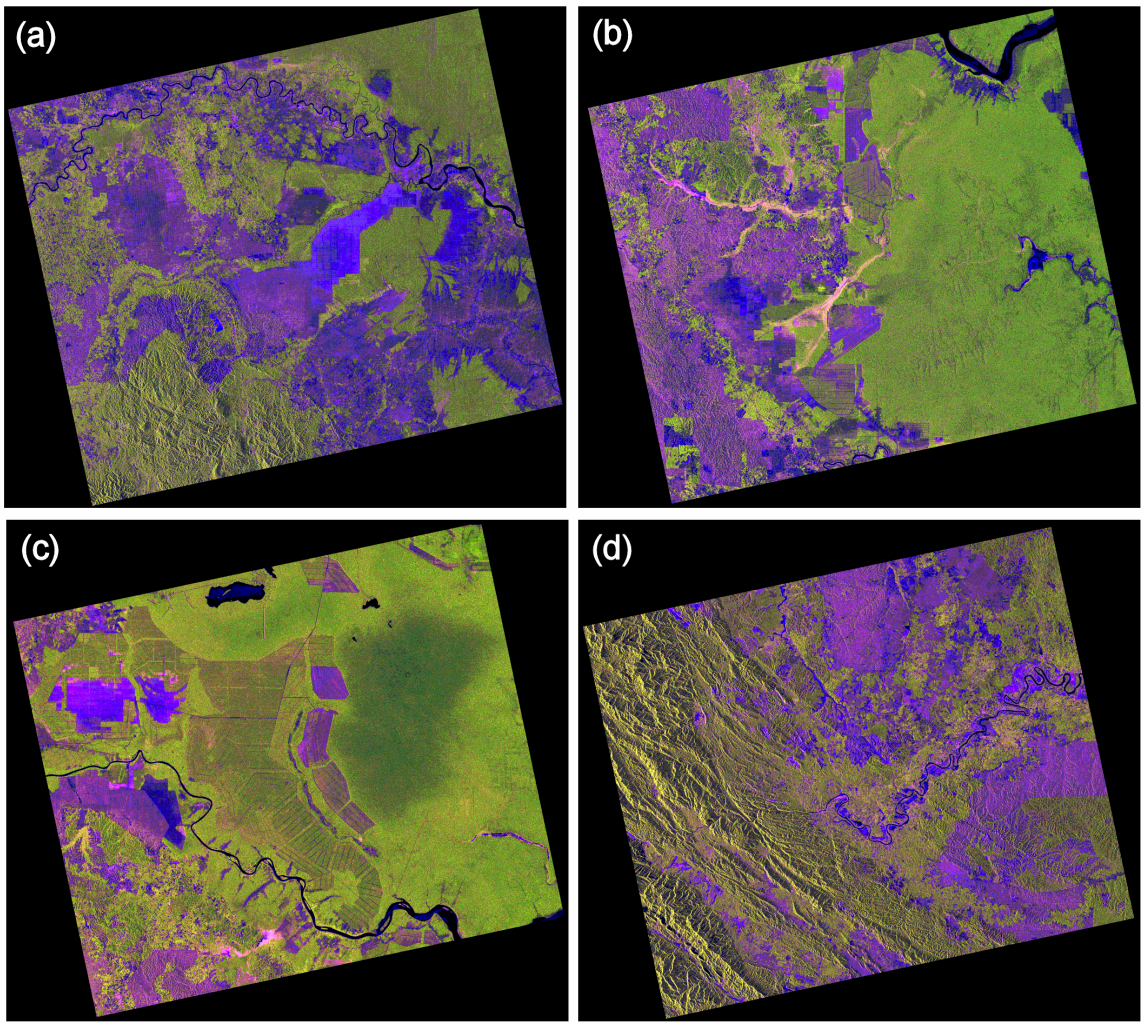

Figure S1. RGB images of the four FBD scenes used. The HH, HV and HH/HV data in the FBD image take the red, green and blue channels respectively. (a) P443-F7170 (28/06/2007); (b) P443-F7180 (28/06/2007); (c) P443-F7190 (28/06/2007)(d) P445-F7170 (01/08/2007).

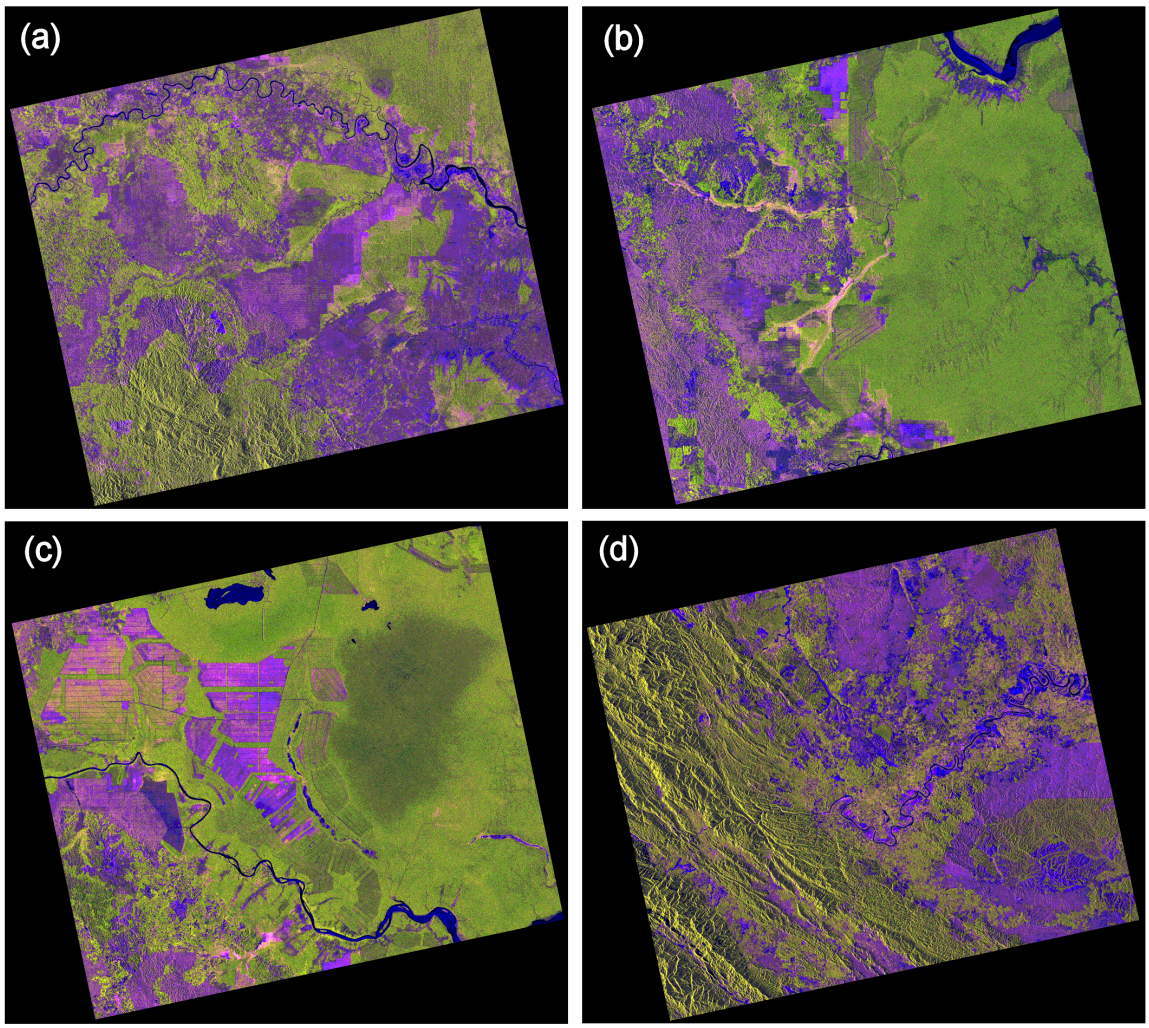

Figure S2. RGB images of the four FBD scenes used. The HH, HV and HH/HV data in the FBD image take the red, green and blue channels respectively. (a) P443-F7170 (30/06/2008); (b) P443-F7180 (30/06/2008); (c) P443-F7190 (30/06/2008)(d) P445-F7170 (03/05/2008).